

Radially transmitted changes in hydraulic and osmotic pressures help explain reversible and irreversible patterns of tree stem expansion

Sebastian Pfautsch¹, John Drake², Mike Aspinwall³, Victor Resco de Dios⁴, Craig Barton¹, Patrick Meir⁵, Mark Tjoelker⁶, David Tissue¹, and Maurizio Mencuccini⁷

¹Western Sydney University

²SUNY College of Environmental Science and Forestry

³Auburn University

⁴Southwest University of Science and Technology

⁵The Australian National University

⁶Western Sydney Univeristy

⁷University of Edinburgh

June 27, 2021

Abstract

It is easy to measure annual growth of a tree stem. It is hard to measure its daily growth. The reason for this difficulty is the microscopic scale and the need to separate processes that simultaneously result in reversible and irreversible stem expansion. Here we present a model that separates reversible from irreversible cell expansion. Our model is novel, because it explains reversible expansion as consequence of longitudinally and, importantly, radially transmitted changes of hydraulic and osmotic pressures in xylem and bark. To capture and quantify these changes, we manipulated daily stem growth by applying a phloem girdle to stems of 9-m tall trees. The model was informed by measurements of radial movement in stem tissues and sap flow before and after and positions below and above the girdle. Additional measurements of whole-crown fluxes of H₂O and CO₂, leaf water potentials, non-structural carbohydrates and respiration were used to document the physiological impacts of girdling. This work sheds new light on the role of radial transport processes underpinning daily growth of tree stems. The model helps explain diel patterns of stem growth in trees.

Radially transmitted changes in hydraulic and osmotic pressures help explain reversible and irreversible patterns of tree stem expansion

Sebastian Pfautsch^{1,2}, John E. Drake^{2,3}, Michael J. Aspinwall^{2,4}, Victor Resco de Dios^{5,6,7}, Craig V.M. Barton², Patrick Meir^{8,9}, Mark G. Tjoelker², David T. Tissue², and Maurizio Mencuccini^{10,11}

¹Urban Studies, School of Social Science, Western Sydney University, Locked Bag 1797, Penrith, NSW 2751, Australia

²Hawkesbury Institute for the Environment, Western Sydney University, Locked Bag 1797, Penrith, NSW 2751, Australia

³Sustainable Resources Management, State University of New York College of Environmental Science and Forestry, 1 Forestry Drive, Syracuse, NY 13210, United States

⁴School of Forestry and Wildlife Services, Auburn University, 602 Duncan Drive, Auburn, AL 36849, United States

⁵School of Life Science and Engineering, Southwest University of Science and Technology, Mianyang, Sichuan 621010, P.R. China

⁶Departament of Crop and Forest Sciences, University of Lleida, Lleida 25198, Spain

⁷Joint Research Unit CTFC-AGROTECNIO-CERCA Centre, Lleida 25198, Spain

⁸School of Geosciences, University of Edinburgh, United Kingdom

⁹Research School of Biology, Australian National University, Canberra, ACT 2601, Australia

¹⁰ICREA, Barcelona 08010, Spain

¹¹CREAF, Cerdanyola del Vallès, Barcelona 08193, Spain

Corresponding Author Sebastian Pfautsch

Phone +61 2 9685 9081

Email s.pfautsch@westernsydney.edu.au

Abstract

It is easy to measure annual growth of a tree stem. It is hard to measure its daily growth. The reason for this difficulty is the microscopic scale and the need to separate processes that simultaneously result in reversible and irreversible stem expansion. Here we present a model that separates reversible from irreversible cell expansion. Our model is novel, because it explains reversible expansion as consequence of longitudinally and, importantly, radially transmitted changes of hydraulic and osmotic pressures in xylem and bark. To capture and quantify these changes, we manipulated daily stem growth by applying a phloem girdle to stems of 9-m tall trees. The model was informed by measurements of radial movement in stem tissues and sap flow before and after and positions below and above the girdle. Additional measurements of whole-crown fluxes of H₂O and CO₂, leaf water potentials, non-structural carbohydrates and respiration were used to document the physiological impacts of girdling. This work sheds new light on the role of radial transport processes underpinning daily growth of tree stems. The model helps explain diel patterns of stem growth in trees.

Key Words

Dendrometer, girdling, mechanistic growth model, non-structural carbohydrates, osmotic potential, radial transport, ray parenchyma, source-sink relationships, tree growth

1. Introduction

Vertical transport of non-structural carbohydrates (NSC) in phloem and water in xylem of tree stems have been the subject of countless investigations. In contrast, radial transport processes remain understudied, and this limits our understanding of day-to-day growth dynamics in trees (Cuny *et al.* 2015; De Swaef *et al.* 2015). The prevailing view is that trees accumulate NSC during the day in leaves and use them to support stem growth during the night when tissues are highly turgid (e.g., Hölttä *et al.* 2010; Steppe *et al.* 2015). This view is supported, at least partly, by time-series data documenting maximum stem expansion during the night in several tree species of the temperate zone of the northern hemisphere. However, examples from other biomes have now shown that the origin of radial movement in tree stems can be far more complex, involving irreversible (i.e., radial growth) and reversible (i.e., radial expansion-contraction) processes that can occur independently or simultaneously, during the day and/or night (e.g., Pfautsch *et al.* 2015a; Mencuccini *et al.* 2017).

At the cellular level, irreversible radial growth (D^G) results from periclinal division of mother cells located inside (sapwood) and outside (phloem) a meristematic region of the secondary cambium (Schrader *et al.* 2004). A combination of exogenous and endogenous factors triggers the formation of primary cell walls.

Subsequently, individual layers of new cell walls undergo biosynthetic processes that lead to densification, dehydration and lignification, which conclude the process of D^G . Not only do sapwood mother cells differentiate more than phloem cells – typically at a ratio of 4:1 to 10:1 in trees (Fromm 2013) – they are also permanently retained as wood, whereas phloem cells are eventually shed. It is widely accepted that NSC are the primary carbon source supporting D^G in trees (e.g., Hartmann and Trumbore 2016; Martínez-Vilalta *et al.* 2016).

In contrast to D^G , reversible stem expansion and contraction is the result of differences in hydraulic pressure and osmotic potential between xylem and capacitive water stores in sapwood and bark (note that bark in this context is the living section of bark that contains both phloem and cambium). The resulting bi-directional transport of water and osmotic substances is mostly organized through transport in rays that provide a functional link between bark and xylem (e.g., Sevanto *et al.* 2011; Pfautsch *et al.* 2015b; Pfautsch 2016). Contraction of stems during daytime and their expansion during night-time, similar to a sine-wave curve (Scenario 1 in Fig. 1), partly results from radial transport processes. It is widely accepted that this fluctuation in radial direction is primarily a result of mobilising and replenishing stored water in xylem, sapwood and bark, following shifts in vertical gradients of hydraulic pressure (e.g., Zweifel *et al.* 2001; Steppe *et al.* 2006; Hölttä *et al.* 2009; Mencuccini *et al.* 2013). Contraction and expansion of sapwood and bark is commonly observed to occur in synchrony, although movement of bark may lag slightly behind that of sapwood as a consequence of the indirect coupling through rays with the transpiration stream inside the xylem (e.g., Sevanto *et al.* 2003, 2011).

Studies of stem diameter changes in *Eucalyptus* species have revealed different, asynchronous patterns. Sapwood of *E. globulus* contracted and bark expanded during the day (Scenario 2 in Fig. 1), which indicated asynchronous patterns driven by strong hydraulic decoupling between xylem and bark (Zweifel *et al.* 2014). Solomon *et al.* (2010) observed a temporal separation of processes related to biosynthesis and lignification of new cell wall materials in *E. globulus*, as well as temporal variation in regulation of genes that encode aquaporins, which facilitate influx of water in expanding, growing cells. These findings provide additional evidence that D^G and reversible expansion and contraction of stems are complex processes that can act at different time scales. An additional asynchronous pattern was observed in stems of *E. saligna* and *E. tereticornis* (Scenario 3 in Fig. 1), where sapwood expanded, and bark contracted during the day (Pfautsch *et al.* 2015a; Mencuccini *et al.* 2017). The two asynchronous patterns do not match widely accepted plant hydraulic modelling of a contraction of sapwood during morning hours as the result of increasingly negative hydraulic pressure in xylem (e.g., Steppe *et al.* 2015). A mechanistic basis for asynchronous radial expansion and contraction of stem tissues has not yet been fully established.

It is technically challenging to simultaneously document dynamic changes in multiple sinks to determine sink strength and preferential use of available carbon resources. Systematic isolation of potential carbon sinks from supply of NSC by using the phloem girdling technique can circumvent this issue. Phloem girdling has been used successfully to investigate carbon dynamics of trees (e.g., Hogberg *et al.* 2001; Binkley *et al.* 2006; Appel *et al.* 2012), and regulation of photosynthesis by turnover of sugars and starch in leaves (Nebauer *et al.* 2011). Importantly, measurements of girdling effects on stems, leaves, NSC metabolism and transpiration markedly increased our understanding of the interrelatedness of water and carbon economies in plants (e.g., De Schepper *et al.* 2011; Sellin *et al.* 2013; López *et al.* 2015).

Assessment of girdling effects on short-term dynamics of radial growth in stems is complex because of the simultaneous appearance of cambial cell development and reversible expansion and contraction of stems caused by hydraulic and osmotic effects. For example, with the onset of transpiration during morning hours, water stored in bark and sapwood can be drawn into xylem, where it mitigates increasingly negative water potentials in conducting vessels. The loss of capacitive water in the bark or sapwood will result in contraction of the affected tissues (e.g., Zweifel *et al.* 2001; Pfautsch *et al.* 2015a). Similarly, osmotically-induced radial fluxes of water can lead to expansion or contraction of bark. Thus, when recording the radial movement of stems at high temporal resolution, several signals are recorded concurrently (Chan *et al.* 2016).

Here, we use phloem girdling to manipulate source-sink relationships in *E. tereticornis* trees and employ point

dendrometers with high temporal and dimensional resolution to document changes in D^G and reversible expansion and contraction of bark and sapwood. However, deciphering the sequence of processes that result in stem growth cannot be achieved by observing effects of girdling alone because of the fundamental links between the carbon and water economies inside trees. It is necessary to also quantify the effects of girdling on carbon assimilation and related changes in the use of NSC, and loss of carbon (C) through respiration (R), but also any effects on transpiration. Girdling has been shown to increase respiratory C loss from tree stems by 45% (Yang *et al.* 2019) and markedly reduce transpiration (Oberhuber *et al.* 2017). We developed a mechanistic model that can disentangle most of these underlying processes, including radial transport of water between bark and xylem. The present work refines previous models (Mencuccini *et al.* 2013, 2017) by including a term for the lateral flux of solutes and the associated changes in osmotic potential between bark and xylem that drive radial viscoelastic changes in tree stems. We hypothesise that daytime increases in osmotic potential in rays lead to sapwood expansion which significantly counter-balances tension-driven contraction in xylem and fibres. The observed high rates of leakage and uptake of soluble sugars by phloem (Epron *et al.* 2016; Furze *et al.* 2018), and the pronounced radial transport of water in the symplast of rays (Pfautsch *et al.* 2015b), support this concept. Use of a wide range of experimental data and output from the improved mechanistic model allowed us to generate empirical evidence of “pathway effects” (*sensu* Sellier & Mammeri 2019) of phloem loading, its impact on D^G at different positions along the vertical stem axis and underlying asynchronous patterns of reversible expansion and contraction of bark and sapwood tissues.

2. Materials and Methods

The experiment took place in May 2014 at the Whole Tree Chamber (WTC) facility of the Hawkesbury Institute for the Environment (Fig. S1), 60 km northwest of Sydney, Australia. Mean annual temperature at the facility is 17 °C and mean annual rainfall is 800 mm. We used six cylindrical and cone-topped whole tree chambers (WTC; 3.25 m diameter, 9.4 m tall) which had climate control units, providing regulation of air temperature (T_{air} , °C), relative humidity (RH, %) and soil water content via irrigation. Aboveground fluxes of water (H_2O) and carbon dioxide (CO_2) inside each chamber were measured automatically using infrared gas analysers (see Drake *et al.* 2016). Belowground gas fluxes were excluded from aboveground water and carbon fluxes by installing an airtight polyethylene barrier 45 cm above the soil surface. A detailed description of design, function and measurement routines of the chambers can be found in Barton *et al.* (2010). Whole-crown fluxes of H_2O and CO_2 inside the chambers were recorded at 15-minute intervals as explained in Barton *et al.* (2010) and Drake *et al.* (2016). Here, we present whole-tree gas fluxes for daytime periods (07:00-16:00 h).

2.1 Environmental monitoring

A weather station was used to record ambient conditions at the Whole Tree Chamber site. The station recorded air T_{air} , relative humidity (RH, %) (HMP45C, Vaisala, Helsinki, Finland) and photosynthetically active radiation (PAR, $\mu\text{mol m}^{-2}\text{s}^{-1}$) (SQ-110, Apogee Instruments Inc., Logan, Utah, USA), which were all stored on a data logger at 1-minute intervals (Logger: CR3000, Campbell Scientific, Garbutt, Australia). We used the formula from Snyder & Shaw (1984) to calculate vapour pressure deficit (VPD, kPa) from measurements of T_{air} and rH. During the experiment, the climate control system of each chamber tracked ambient conditions based on measurements collected by the weather station.

2.2 Trees and phloem girdle

One *Eucalyptus tereticornis* tree was grown at ambient T_{air} in each of the 6 chambers for 17 months (December 2012 – May 2014). Trees grew in 25 L pots for three months before transplanting the seedlings into the chamber soil (see Drake *et al.* 2016). On the day of girdling (16 May 2014), trees were 8.0 to 9.3 m tall and basal stem diameter ranged from 78 to 103 mm (Table 1). Trees were phloem girdled by removing a 5 cm wide collar of bark (6-8 mm thick) from the stem at 600-700 mm above the soil surface (see Fig. S1). Dehydration of the exposed sapwood was minimised by wrapping wet paper towels (kept moist daily) and plastic foil around the injured stem. Girdled trees remained well-watered in the WTCs until 26 May 2014, when they were destructively harvested.

Prior to girdling, total leaf number of each tree crown was determined by manual counting (see Drake *et al* . 2016). At the end of the experiment, we collected a subset of 300 leaves from each tree crown to estimate the average area of leaves (Li3600C Area Meter, Li-COR, Lincoln, USA). Multiplying this value with the total number of leaves produced a good estimate for total leaf area of each tree, which was used to express H₂O and CO₂ fluxes on a leaf area basis using a ‘big leaf’ type approach (e.g., McNaughton & Jarvis 1991).

2.3 Leaf water potential measurements

Measurements of leaf water potential were required to develop the modelling routine for predicting radial movement in stems (see section *Stem hydraulic model* below). Three leaves from the top crown region of all six trees were collected during midday of 20 February, 4 March, 26 March, 24 April and 14 May 2014. Immediately after collection, leaves were placed in plastic bags that contained moist paper towels. Plastic bags were transferred to the laboratory in a dark icebox. Their water potential was measured within 30 minutes after collection using a pressure chamber (1505D, PMS Instrument Company, Albany, USA). Results from these measurements are provided as Supporting Information (Table S2).

2.4 Sap flow

Two sap flow units (HeatPulser, Edwards Industries, Otaki, New Zealand) were installed 10 cm below each pair of dendrometers (base and top positions of all six trees). A drill guide was used to ensure axial alignment of the three Teflon probes from each unit. Measurement probes were placed to record heat velocity in the outer sapwood (1 cm depth); heater probes were fully inserted. Positions of all probes were fixed by tying the probe hubs to the stem. Care was taken that the probes were not installed in reaction wood or near old branches.

Sap flow data were logged every 15 min (CR1000, Campbell Scientific, Logan, USA). Sap flow units were installed in January 2014. Bark depth and stem diameter were measured once every month at each position to calculate the increase in sapwood area over the duration of the experiment. Hourly sap flow data are shown in Supporting Information (Fig. S3) and were calculated based on sapwood area measurements for the month of May. Macroscopic analyses of wood discs showed no signs of heartwood formation, so it was concluded that the entire sapwood area was conducting water (i.e. sapwood = xylem). Sap flow measurements were only used to calibrate our *Stem Hydraulic Model* and are not reported here in detail.

2.5 Metabolite analyses

Non-structural carbohydrates (NSC) in leaves and bark are predominately present as starch (St) and soluble sugars (Ss) (Hartmann & Trumbore 2016). To determine if girdling affected the concentration of St and/or Ss, we collected three fully expanded leaves from the upper and lower crown of each tree immediately before girdling (10:00 h, 16 May) and 9 days after girdling at the end of the experiment (10:00 h, 25 May). No branches were present below the girdle, thus leaves sampled from the lower crown originating from immediately above the girdle. Bark tissue (3 cm²) was sampled at the same time from the main stem close to the installation sites of sap flow sensors and dendrometers at the base and top of stems. Immediately after collection, samples were snap-frozen in liquid N and stored at -80 °C prior to further processing.

Prior to extractions, leaves and bark samples collected prior and during the girdling experiment were dried at 70 °C to a constant weight and ground to a fine powder using a ball mill. Concentration of St and Ss was determined using a procedure adapted from Tissue and Wright (1995) that required 15-20 mg of sample material. In a first step, Ss were washed out of solids using a methanol-chloroform-water solution (12:5:3 v/v). In the following step, St was extracted from solids using perchloric acid (35% v/v). Concentrated sulphuric acid was then used to hydrolyse both Ss and St to glucose, before addition of phenol induced a colorimetric reaction. Finally, absorbance of glucose-phenol solutions was measured at 490 nm in a photometer (DU 800 Spectrophotometer, Beckman Coulter, Sydney, Australia), and readings were converted to quantities of Ss and St using a simple mathematical approach.

2.6 Respiration

We assessed girdling effects on respiratory physiology by measuring leaf, branch wood, and whole-crown respiration three days before (13 May) and six days after the trees were girdled (22 May). Two branches were selected at random for each chamber on each date, and branches were detached in the evening by cutting at the stem insertion point. All leaves were removed prior to cutting each branch in to 10 cm long segments. All segments of a single branch were placed into a large gas exchange chamber (3010-GWK1, Heinz Walz GmbH, Effeltrich, Germany) connected to an infrared gas analyser (IRGA; LI 6400-XT, LiCor, Lincoln, NE, USA). The chamber temperature was controlled such that the tissue temperature was 15 °C (± 0.5). The CO₂ concentration of the reference cell was 400 ppm and the flow rate was 700 $\mu\text{mol s}^{-1}$. The flow rate was selected to cope with high amounts of water vapour released from stem segments. We recognise that sampling may have affected respiration rates or released CO₂ dissolved in the xylem. However, measuring respiration of detached plant organs is a standard approach (e.g., Poorter *et al.* 1990; Tjoelker *et al.* 1999, 2005; Comas & Eissenstat 2002; Drake *et al.* 2016, 2017), and we expect any sampling effects to be systematic across dates and not affect our ability to detect girdling effects.

The leaves from each branch were mixed and three leaves were selected at random; the respiration rate of these three leaves were measured as a composite sample using a large, opaque leaf cuvette (Li-6400-XT with Li-6400-22 conifer chambers; Licor). The block temperature was controlled such that the leaf temperature was 15 °C (± 0.5). The CO₂ concentration of the reference cell was 400 ppm and the flow rate was either 350 or 500 $\mu\text{mol s}^{-1}$, depending on moisture levels. This flow rate was lower compared to that used for stem segments, as less water vapour was released by the leaves. Leaves and branches were dried and weighed, and respiration rates were expressed per unit dry mass. Note that the pre-girdling leaf and branch respiration measurements were presented in Drake *et al.* (2016). The post-girdling data have not previously been published.

After the two branches were removed for the pre-girdling branch and leaf respiration measurement (13 May), we measured respiration of the entire aboveground biomass of each tree. For these measurements, each whole-tree chamber was manually transformed into a closed system that excluded soil and the rate of CO₂ accumulation within the chamber airspace was measured every minute. The whole-tree chamber environmental controls were used to maintain the air temperature in all chambers at 15 °C. The rate of CO₂ efflux from the entire crown was calculated as in Drake *et al.* (2016). Note that these measurements reflect the combined respiratory activity of leaves, branches, and the stem. These measurements were collected during night-time. The total mass of leaves, branches, and stem wood was measured via a full destructive harvest on 26 May 2014. All leaves, branches, and stem wood were manually separated for each tree, dried, and weighed. The total sum of leaf, branch, and stem wood dry mass was used to express the whole-tree respiration measurements per unit total aboveground mass. We assume that total tree mass did not change appreciably over the 13 days separating the first crown respiration measurement and the tree harvest.

2.7 Dendrometers

Linear variable displacement transducers were used as high-precision point dendrometers (ZN11, Zweifel Consulting, Hombrechtikon, Switzerland). Technical information about the sensors and their mounting to tree stems can be found at Zweifel *et al.* (2014). Pairs of dendrometer units were installed at 60 cm above ground (termed ‘base’) and at a position where stem diameter was 3 cm (termed ‘top’), resulting in a total of 24 mounted units. Installation height of dendrometers at top varied among trees (Table 1), but distance between base and top was always more than 2.5 m. Pistons of the dendrometers were positioned directly on bark and sapwood. For the latter, we cut a small bark window (1 cm²) using a chisel. Bark windows were flushed with deionised water after carefully scraping cambial cells from the outer sapwood. Once cleaned and padded dry, the tip of a dendrometer plunger was positioned directly onto sapwood and bark windows were sealed using silicone grease to prevent drying of exposed stem tissues.

Measurements recorded on sapwood were used to calculate the amplitude of radial movement in xylem (D_x). Subtracting D_x from measurements collected on bark isolates the bark signal representing radial movement generated by reversible (cambium and phloem) and irreversible (formation of wood) radial movement. In a second step, we separated radial movement related to the two co-occurring processes. First, we calculated the

difference between maximal and minimal dimensions during a single diurnal cycle to represent the reversible, bark-driven proportion of the total movement (D_b) only. Next, we assessed the difference between two consecutive minimum expansions measured on bark to determine irreversible cambial growth ($D^{G_{\text{empir}}}$). These are the simplest mathematical procedures when analysing data from simultaneous measurements on sapwood and bark using point dendrometers (Mencuccini *et al.* 2017). We note that the term $D^{G_{\text{empir}}}$ is a composite measure that contains hydraulic and osmotic signals that can mask true irreversible cambial growth. See section ‘*Stem Hydraulic Model*’ below for further details.

To assess the effect of girdling on dimensional changes of live bark and xylem, we zeroed dendrometer readings against the measurement recorded at midnight of 5 May 2014 (pre-girdling) and 19 May (post-girdling). Time-series data (base and top positions of all six trees) from 6-10 May was used as baseline data, measurements from 20-24 May were used to assess how girdling affected D_x, D_b and $D^{G_{\text{empir}}}$. The prefix ‘d’ will be used to signify ‘change in’ (e.g., dD_x is the dimensional change in radial direction in xylem).

2.8 Stem hydraulic model

The model developed by Mencuccini *et al.* (2017) separates the relative dimensional changes of D_b caused by irreversible cambial growth (D^G) (plastic growth in the terminology of Cosgrove 2005) from those due to reversible elastic changes. The latter are the result of transpiration-driven, negative hydraulic pressure changes in xylem ($D_b^{\Psi\Pi,\xi}$) and changes in the bark osmotic pressure ($D_b^{\Psi\Pi,\beta}$) caused by shifts in the balance between phloem carbohydrate supply and radial growth. Note that here and later on in the text, variables $D_b^{\Psi\Pi,\xi}$ and $D_b^{\Psi\Pi,\beta}$ must be read as the component of bark diameter D_b affected by changes in xylem pressure potential ΨP_x and bark osmotic potential $\Psi\Pi_b$, respectively. The same applies for the D_x variables presented later on. However, the Mencuccini *et al.* (2017) model did not account for lateral solute fluxes between bark and xylem via rays. That is, whereas $D_b^{\Psi\Pi,\xi}$ (i.e., transpiration-driven) does account for lateral water fluxes, $D_b^{\Psi\Pi,\beta}$ (osmotic pressure-driven) only accounts for osmotic changes within bark. Here, we expand the model to incorporate an additional lateral osmotic transfer function; please refer to Supporting Information (Method S1, Table S1) and Mencuccini *et al.* (2017, 2013) for full details of the model.

Here we assumed that:

Radial transfer of osmotica between bark and xylem determines reversible changes of bark thickness.

The reversible radius change of xylem is the sum of two independent processes, one driven by the shrinkage/expansion of dead conduits and live cells under negative pressure ($D_x^{\Psi\Pi,\xi}$) and one driven by shrinkage/expansion of the live xylem parenchyma cells (i.e., rays) caused by radial solute transport to/from bark ($D_x^{\Psi\Pi,\beta}$) with subsequent impacts on accumulation/release of symplastic water in/from rays.

3) The rate of radial solute transfer to/from bark is identical in magnitude, but opposite in sign, to the rate of radial solute transfer from/to xylem. This assumption is only approximately correct, since a fraction of the solutes transported radially from bark into xylem-bound rays will form the building blocks of irreversible growth in the cambial growth zone.

4) No net transfer from soluble to non-soluble carbohydrates *vice versa* during this transfer.

Hosted file

image1.emf available at <https://authorea.com/users/92525/articles/528006-radially-transmitted-changes-in-hydraulic-and-osmotic-pressures-help-explain-reversible-and-irreversible-patterns-of-tree-stem-expansion>

The final expression for change in bark thickness is:

Hosted file

image2.emf available at <https://authorea.com/users/92525/articles/528006-radially-transmitted-changes-in-hydraulic-and-osmotic-pressures-help-explain-reversible-and-irreversible-patterns-of-tree-stem-expansion>

irreversible-patterns-of-tree-stem-expansion

(1)

Reversible changes in bark thickness depend on three processes. First, changes in bark hydraulic capacitance (component 1), expressed by the symbol $D_b^{\Psi\Pi,\xi}$ in the text; second, changes in bark osmotic concentration (component 2) caused by lateral solute fluxes, i.e. $D_b^{\Psi\Pi,\beta}$; third, xylem conduit diameter response to xylem tension (component 3), i.e. $D_x^{\Psi\Pi,\xi}$. The first two processes are driven by the radial fluxes, respectively, of water and solutes to and from the xylem into the bark. The third component is the result of a balancing act between soil water availability, atmospheric dryness and stomatal regulation of water loss at the leaf. Component 1 in Eqn. (1) is derived from Mencuccini *et al.* (2013). Therefore, the term marked as component 2 in Eqn. (1) above gives the net fraction of the changes in bark osmotic concentration that depends directly on the corresponding changes in xylem osmotic concentration. α , β and γ are defined as in Mencuccini *et al.* (2017):

Hosted file

image3.emf available at <https://authorea.com/users/92525/articles/528006-radially-transmitted-changes-in-hydraulic-and-osmotic-pressures-help-explain-reversible-and-irreversible-patterns-of-tree-stem-expansion>

Hosted file

image4.emf available at <https://authorea.com/users/92525/articles/528006-radially-transmitted-changes-in-hydraulic-and-osmotic-pressures-help-explain-reversible-and-irreversible-patterns-of-tree-stem-expansion>

, (2)

with * indicating the measurement at the beginning of the time series, taken as a reference. Once the predicted elastic changes in bark thickness obtained via Eqn. (1) are subtracted from observed bark thickness changes, D^G is obtained using the differential-evolution minimization algorithm described in Mencuccini *et al.* (2017). This final step separates irreversible growth D^G from the remaining component of elastic changes, i.e., local changes in bark osmotic pressure that are caused by shifts in the balance between phloem carbohydrate supply and radial growth. For clarity, we introduce the term D^{G+} to indicate the novel capacity of our model to isolate not only vertical, but also small, yet physiologically important radial processes related to hydraulic and osmotic adjustments that impact the reversible expansion dynamics in live bark and xylem. D^{G+} supersedes D^G . Cumulative daily increments of D^G_{empir} and D^{G+} were calculated to assess the fit between our empirical dendrometer measurements with model predictions for irreversible stem growth.

2.9 Statistical analyses

One-way repeated-measures analysis of variance (RM ANOVA) was used to assess the effect of girdling on respiration of leaves and branches. We used linear mixed effect modelling to assess differences in St and Ss in leaves and bark before and after girdling (fixed effects), accounting for tree number, sample position and sampling date (random effects). Linear mixed effect modelling was also used to account for tree number, sample position and sampling date (random effects) when assessing differences in D_x and D_b prior and after girdling (fixed effects). Student's t-tests were used to assess differences in D^{G+} before and after girdling. We report the marginal R^2 (proportion of total variance explained through fixed effects) and conditional R^2 (proportion of total variance explained through fixed and random effects) of the mixed effect model.

Regression analyses were used to determine the effect of girdling on the relationships between whole-tree fluxes of H_2O and CO_2 and environmental drivers, namely PAR, T_{air} and VPD prior to and after girdling. Single factor ANOVA and Fisher's LSD test were used to assess the effect of sample location (base, top) on the daily amplitude of expansion and contraction in D_x , D_b , and D^G_{empir} . These tests also included comparing pre-girdle (6 to 10 May) to post-girdle (20 to 24 May) measurements. Violation of the condition of homogeneity of variance of these data was tested (Barlett's chi-square) and rejected in all cases as $p > 0.05$.

3. Results

3.1 Environmental conditions

The Whole Tree Chambers that housed our girdled trees tracked ambient environmental conditions. From 6-25 May, cloud cover was minimal, resulting in clear diurnal patterns of PAR with maxima around 1150 $\mu\text{mol m}^{-2} \text{s}^{-1}$ (Fig. S2). During the experimental period, mean daytime air temperature increased slightly from 17.3 °C (6 to 15 May) before to 18.8 °C (17 to 24 May) after trees were girdled. At the same time, mean daytime VPD rose from 0.7 kPa to 0.8 kPa and mean maximum VPD increased from 1.5 kPa to 2.2 kPa.

3.2 Effect of girdling on NSC in leaves and bark

Mean NSC concentration of leaf tissues collected pre-girdling (Fig. 2a) and post-girdling (Fig. 2b) was around 170-200 $\text{mg g}^{-1}\text{DW}$ with a range of 140-280 $\text{mg NSC g}^{-1} \text{DW}$. The ratios of Ss to St shifted slightly from 1:1.5 at pre-girdling to 1:1.9 at post-girdling. Girdling caused a significant decline ($p < 0.01$) in Ss of leaves, compared to pre-girdling, at the base (74.24 $\text{mg g}^{-1} \text{DW} \pm 6.71$ to 64.35 $\text{mg g}^{-1} \text{DW} \pm 7.17$; ± 1 Standard Deviation) and top crown positions (72.61 $\text{mg g}^{-1} \text{DW} \pm 8.42$ to 62.87 $\text{mg g}^{-1} \text{DW} \pm 9.83$) (Fig. 2a, b). Concentrations of St differed significantly ($p > 0.001$) between leaves from the base and top crown positions at pre-girdling (Fig. 2a), but not at post-girdling (Fig. 2b).

Bark generally contained less total NSC than leaves ($< 150 \text{ mg g}^{-1} \text{DW}$), largely due to a smaller pool of St (Fig. 2c, d). Prior to girdling, pools of St and Ss in bark from the base and the top of the stem did not differ (Fig. 2c). However, girdling reduced St below the girdle by 23% (base: 57.92 $\text{mg g}^{-1} \text{DW} \pm 6.76$; top: 74.89 $\text{mg g}^{-1} \text{DW} \pm 2.97$) and Ss by nearly 50% (base: 25.84 $\text{mg g}^{-1} \text{DW} \pm 6.71$; top: 48.90 $\text{mg g}^{-1} \text{DW} \pm 14.14$) compared to above the girdle (Fig. 2d). Overall, the ratio of Ss:St shifted from 1:1.4 at pre-girdling to 1:2.3 at post-girdling. Similar to leaves, girdling had a much stronger effect on the pool of Ss compared to St in bark tissue. Notably, bark below the girdle contained the lowest concentrations of both Ss and St (Fig. 2d).

3.3 Effect of girdling on whole-tree H_2O and CO_2 fluxes

Girdling reduced whole-tree fluxes of H_2O and CO_2 (Fig. 3) and increased dark respiration of woody above-ground biomass (Table 2). Prior to girdling, mean hourly CO_2 fluxes showed a moderately strong positive and relationship with PAR ($R^2 = 0.68$) with a typical curvilinear trajectory that indicates saturation of CO_2 uptake with increasing PAR as consequence of limited photosynthetic capacity (Fig. 3). Average daytime CO_2 fluxes were 0.76 $\text{g m}^{-2} \text{h}^{-1}$ on a leaf-area basis. After girdling, this saturating relationship remained, albeit slightly weaker ($R^2 = 0.56$), and average daytime CO_2 fluxes noticeably declined ($p = 0.009$) to 0.59 $\text{g m}^{-2} \text{h}^{-1}$. Under the same light intensity of 1000 $\mu\text{mol m}^{-2} \text{s}^{-1}$ the CO_2 flux dropped from 1.15 $\text{g m}^{-2}\text{h}^{-1}$ pre-girdling to 0.73 $\text{g m}^{-2}\text{h}^{-1}$ post-girdling (Fig. 3a). The same effect was observed for H_2O fluxes, where girdling significantly ($p < 0.001$) reduced whole-tree transpiration at similar PAR intensities (Fig. 3b).

There was no effect of T_{air} (and VPD) on whole-tree C uptake (Fig. 3c, e). In contrast, transpiration was significantly ($p < 0.001$) and positively dependent on T_{air} (and VPD). However, despite warmer mean T_{air} and higher VPD in the days following girdling, whole-tree transpiration declined in response to girdling ($p < 0.001$) (Fig. 3d, f). Average daily whole-tree transpiration declined from 92.4 $\text{ml m}^{-2}\text{h}^{-1}$ pre-girdling to 68.7 $\text{ml m}^{-2}\text{h}^{-1}$ post-girdling. At VPD of 1 kPa, average H_2O fluxes were around 120 $\text{ml m}^{-2}\text{h}^{-1}$ prior to girdling and 70 $\text{ml m}^{-2}\text{h}^{-1}$ after girdling.

Dark respiration of leaves was not affected by girdling and remained around 3.40 $\text{nmol CO}_2 \text{ g}^{-1}\text{s}^{-1}$ (Table 2). In contrast, dark respiration of branch tissues, following girdling, increased by 42% ($p < 0.001$) from 1.33 $\text{nmol CO}_2 \text{ g}^{-1}\text{s}^{-1}$ (± 0.25) to 1.89 $\text{nmol CO}_2 \text{ g}^{-1} \text{s}^{-1}$ (± 0.29). Girdling also increased dark respiration of the whole aboveground biomass by 21%, but very large variation among trees (2.20-3.69 $\text{nmol CO}_2 \text{ g}^{-1} \text{s}^{-1}$) meant that this increase was statistically not significant $p = 0.10$.

3.4 Effect of girdling on radial dynamics in bark and xylem

Phloem girdling markedly impacted radial fluctuations in xylem (dD_x) and bark tissues ($dD_b + dD^{G_{\text{empir}}}$) below and above the girdle (Fig. 4). Prior to girdling (6-10 May), average dD_x was $22.6 \mu\text{m d}^{-1} (\pm 5.0)$ at the base and $22.2 \text{ d}^{-1} \mu\text{m d}^{-1} (\pm 7.9)$ at the top of trees. $dD_b + dD^{G_{\text{empir}}}$ was nearly four times larger compared to dD_x , measuring $76.8 \mu\text{m d}^{-1} (\pm 29.8, \pm 1 \text{ SD})$ at the base and $71.8 \text{ d}^{-1} \mu\text{m d}^{-1} (\pm 13.5)$ at the top (Fig. 4a, b). Importantly, and independent of girdling, the dynamic changes of dD_x and $dD_b + dD^{G_{\text{empir}}}$ were asynchronous, whereby dD_x exhibited the largest expansion around 14:00 h when $dD_b + dD^{G_{\text{empir}}}$ reached its minimum.

Following girdling (20-24 May), dD_x at the top of stems (above the girdle) remained unchanged ($21.9 \mu\text{m d}^{-1} \pm 7.9$), but significantly declined below the girdle ($13.2 \mu\text{m d}^{-1} \pm 9.7$; $p < 0.001$) (Fig. 4c, d). Girdling slightly increased $dD_b + dD^{G_{\text{empir}}}$ above the girdle ($82.3 \mu\text{m d}^{-1} \pm 26.0$) while it was reduced by more than half below the girdle ($33.5 \mu\text{m d}^{-1} \pm 10.7$; $p < 0.001$). $dD^{G_{\text{empir}}}$ was similar at both measurement positions (base: $49.5 \mu\text{m d}^{-1} \pm 29.7$; top: $51.6 \text{ d}^{-1} \mu\text{m d}^{-1} \pm 17.6$) before trees were girdled. Post-girdling, $dD^{G_{\text{empir}}}$ ceased at the base ($0.2 \mu\text{m d}^{-1} \pm 8.5$) yet slightly increased at the top ($80.1 \mu\text{m d}^{-1} \pm 28.9$).

Interpolated cumulative $D^{G_{\text{empir}}}$ (empirical data based on daily minima) as well as modelled D^{G+} at the base of trees showed a continuous increase of plastic growth prior to girdling with no distinct diurnal pattern (Fig. 4e). During daytime (7:00-19:00 h) mean $D^{G_{\text{empir}}}$ was 52% (± 4.5) and D^{G+} was 50.3% (± 2.7) of total plastic growth realised during a 24-hour cycle (i.e., 7:00-7:00 h). As indicated earlier, plastic growth below the girdle ceased entirely, thus no diel patterns were identifiable. At the top of trees, plastic growth was also continuous before the girdle was applied, yet at this position $D^{G_{\text{empir}}}$ and D^{G+} showed a distinct diel cycle with high plastic growth during the day (Fig. 4f). Between 7:00 h and 19:00 h, $D^{G_{\text{empir}}}$ accounted for 77.2% (± 6.8) and D^{G+} for 77.6% (± 1.0) of total plastic growth within the 24-hour cycle. After trees were girdled, this proportion declined to 62.5% for $D^{G_{\text{empir}}}$ and 71.9% for D^{G+} , retaining a clear diurnal rhythm of high plastic growth during the day and lower plastic growth during the night.

Our improved model reproduced the magnitude of plastic growth, stripped of hydraulic and osmotic signals (D^{G+}), well for the base and top measurement positions, and also before and after girdling when compared to $D^{G_{\text{empir}}}$ (Fig. 5). During the 5-day interval before girdling, average cumulative $D^{G_{\text{empir}}}$ was $258.2 \mu\text{m}$ at the base and $256.2 \mu\text{m}$ at the top. Model predictions for the same time interval were similar at the base ($287.2 \mu\text{m}$), but slightly higher at the top ($346.3 \mu\text{m}$). After girdling of trees, the improved model matched empirical measurements well, reflecting the collapse of growth below the girdle and an increase of D^{G+} at the top (Fig. 5).

Separating $\frac{dD_b^{\text{TOT}}}{dt}$ into components 1, 2 and 3 using empirical measurements from dendrometers, sap flow, leaf water potential and environmental information allowed us to separate simultaneously occurring hydraulic (Fig. 6) and osmotic processes (Fig. 7) in live bark, the cambial growth zone and xylem during different parts of the diel cycle. First, model outputs documented systematic fluctuations in dD_b and dD_x in response to diel changes in hydrostatic pressure in the xylem (Fig. 6a, b). With the onset of transpiration in the morning, pressure potential in the xylem ($dD_x^{\Psi_{\text{II}}, \xi}$) declined, leading to a small (approx. $3 \mu\text{m}$) but systematic contraction of sapwood. The increasing negative pressure in xylem vessels was transduced via rays into the live bark, where after a short lag time capacitive water stores began to empty water into the xylem, leading to a large contraction of live bark tissue ($dD_b^{\Psi_{\text{II}}, \xi}$). Following peak transpiration during midday (see Fig. S3), negative pressure in xylem eased, yet capacitive water continued to be drawn from live bark tissue leading to further contraction of live bark, leaving a total daytime contraction of up to $60 \mu\text{m}$. With the onset of darkness, transpiration rates were low, allowing $dD_x^{\Psi_{\text{II}}, \xi}$ to fully recover and remain largely unchanged during the night. At the same time, capacitive stores were recharged leading to an increase of $dD_b^{\Psi_{\text{II}}, \xi}$. Prior to girdling, the magnitude of these hydrostatic processes did not vary between the measurement positions, producing a sine-type oscillation of $dD_b^{\Psi_{\text{II}}, \xi}$.

After trees were girdled, the amplitude of $dD_x^{\Psi_{\text{II}}, \xi}$ and $dD_b^{\Psi_{\text{II}}, \xi}$ markedly declined (Fig. 6c, d). $dD_x^{\Psi_{\text{II}}, \xi}$ was reduced to less than $1 \mu\text{m}$ while its distinct transpiration-driven phases of decline, recovery, and steady-state, remained below and above the girdle. The principal sine-wave pattern of viscoelastic changes in live bark also remained, albeit reduced from 60 to around $20 \mu\text{m}$ after girdling and at both measurement

positions. However, model outputs indicated that girdling caused $dD_b^{\Psi\Pi,\xi}$ below the girdle to deviate from the oscillating pattern around zero to one that was increasingly positive (Fig. 6c), indicating a ‘swelling’ of live bark tissue. This was not observed for $dD_b^{\Psi\Pi,\xi}$ above the girdle.

Prior to girdling, our model showed a simultaneous decline in $dD_b^{\Psi\Pi,\xi}$ (Fig. 6) and $D_x^{\Psi\Pi,\xi}$ (Fig. 7a, b), with similar dimensional change at the base (up to 60 μm) but not the top of trees (15-20 μm). Similar to the oscillating sine-pattern of $dD_b^{\Psi\Pi,\xi}, D_x^{\Psi\Pi,\xi}$ at the base of trees recovered overnight, peaking during early morning. However, $D_x^{\Psi\Pi,\xi}$ at the top of trees showed no recovery during the night, but a sharp increase during the early morning before and also after trees were girdled. This pattern was very similar to dendrometer measurements of D_x shown in Fig. 4b and 4d. Finally, expansion of live bark as result of changes in osmotic pressure within this tissue ($D_b^{\Psi\Pi,\beta}$) peaked at the end of every day before girdling at the base and top of trees (Fig. 7c, d). After girdling, these peaks disappeared below the girdle and $D_b^{\Psi\Pi,\beta}$ steadily declined, showing that expansion of D_b was increasingly less driven by osmotic pressure gradients. The opposite trend, a constant increase in $D_b^{\Psi\Pi,\beta}$ was observed above the girdle. At both positions, the typical late afternoon peak observed prior to girdling had disappeared post-girdling.

Our mixed effect model, that accounted for more than one distinct source of variability, was able to explain a large proportion of uncertainty (conditional R^2 was 0.47 before and 0.40 after girdling; marginal R^2 was 0.51 before girdling and 0.47 after girdling; Table 3). The observed dimensional changes in D_x and D_b resulting from viscoelastic changes in live bark and phloem, as well as changes in patterns of D^{G+} are in agreement with effects associated with reduced transpiration (Fig. S3) and changes in the concentration of NSC that affect physiological and osmotic dynamics (Fig. 1), below and above the girdle.

4. Discussion

Here we have assessed the two most critical transport systems in trees, xylem in sapwood and phloem in bark, as one tightly interconnected system. This approach is supported by previous experimental work that highlighted the role of wood rays as a radial link between the two transport systems (Pfausch *et al.* 2015b; Mencuccini *et al.* 2017). By refining our Stem Hydraulic Model (Mencuccini *et al.* 2017) through incorporation of terms for viscoelastic changes driven by pressure potential of the xylem and osmotic potential exerted by live bark, we were able to accurately isolate diel patterns of irreversible radial growth (D^{G+}) from asynchronous dimensional changes in bark and sapwood. The resulting patterns of D^{G+} showed high rates of wood growth during the day, which stand in contrast to the paradigm that radial growth of stems mostly occurs during the night (Steppe *et al.* 2015). Moreover, by girdling trees, we were able to untangle the effects of hydraulic and osmotic pressure gradients on radial movement of bark and sapwood. Our observed and modelled dimensional changes of tree stems progress recent theoretical work on source-sink relationships (Sellier & Mammeri 2019). Specifically, we were able to quantify dimensional radial expansion and contraction of tissues driven by diurnal oscillations of osmotic pressure potential in live bark and xylem. Further, we identified that D^{G+} close to the source of loading (treetop) followed a pronounced diel pattern of high growth during the day and low growth during the night, compared to continuous increase of D^{G+} further away from the source of loading (base). These growth patterns have now been shown to co-occur simultaneously in eucalypt trees, providing the first empirical evidence for the suggested pathway effects of phloem loading with a stabilising function of NSC supply to distant sinks (Sellier & Mammeri 2019).

4.1 Impact of girdling on H₂O and C economy

Despite higher air temperatures and greater VPD during the post-girdling period, water use of the girdled trees declined. Reductions in transpiration have been observed in other tree girdling experiments and were attributed to feedback responses in Photosystem II (e.g., Sellin *et al.* 2013), photoinhibition due to high concentrations of leaf NSC (e.g., Lopez *et al.* 2015) and also secondary responses unrelated to photosynthesis and NSC (e.g., Asao & Ryan 2015). However, plant material in these earlier studies was kept under identical environmental conditions before and after application of the girdle. In the current study, girdled trees reduced water use under environmental conditions that should stimulate the opposite, and without any noticeable accumulation of NSC in leaves. This points towards another possible chain of events triggered by girdling.

More than 50 years ago, Kurtzman Jr. (1966) suggested that phloem girdling will lead to a reduction in conductive sapwood area as a result of vessel embolism. Since then, studies have investigated how removal of phloem tissue impacts water transport in xylem with some showing a reduction (e.g., Salleo *et al.* 2004; Zwieniecki *et al.* 2004; Tombesi *et al.* 2014), while others did not (e.g., Domec & Pruyn 2008). However, none of these studies assessed if girdling changed the radial pattern of sap flow, which often displays a declining gradient from outer to inner sapwood. One study has directly assessed changes in this radial gradient using dye injections and showed that girdling had the largest impact on conductivity of the outer sapwood (Ueda *et al.* 2014). Combining the results of Ueda *et al.* with (a) the reduction in water use under higher VPD, (b) the absence of accumulation of NSC in leaves and (c) the strong water to air pressure gradient at the surface of exposed sapwood opens the possibility that girdling replaced water with air in rays and other capacitive stores of water in the outer sapwood. This effect would agree with Fick’s second law of diffusion of water in wood (Avramidis 2007). The connection of rays to outer xylem vessels has been documented empirically (Pfautsch *et al.* 2015b), and anatomical analyses have shown that sapwood of *E. tereticornis* can have more than 700 rays mm⁻² (Treydte *et al.* 2021). This evidence points towards pronounced capacity of radial access to xylem vessels. Once rays are air-filled, the negative pressure in vessels would draw air bubbles into the transpiration stream leading to embolism. Experiments using a combination of stem girdling and x-ray or magnetic resonance tomography could be used to validate this interpretation. Regardless of potential effects from embolised vessels on transpiration, the girdling treatment helped separating hydraulic and osmotic processes to validate D^{G+} and increased our fundamental understanding of xylem-phloem interactions.

Increasing embolism in xylem vessels helps explain the observed reduction in whole tree transpiration, especially under rising VPD. Under these conditions, leaf water potentials would decline and reduce stomatal conductance. This sequence of responses to girdling is supported by the decline in whole-tree C uptake. In contrast to other studies (e.g., Johnsen *et al.* 2007; Maier *et al.* 2010; Lopez *et al.* 2015), NSC did not accumulate in leaves of *E. tereticornis*. Moreover, girdling did not lead to higher rates of R in leaves. These results imply that girdling reduced assimilation of carbohydrates, but at least over the few days after girdling, loading of soluble sugars into the phloem continued. The lower rates of assimilation help explain the small yet significant decline of soluble sugars in leaves after girdling.

Girdling of *E. tereticornis* trees resulted in accelerated D^{G+} above and collapse of D^{G+} below the girdle. Further, girdling accelerated rates of R in stems and branches but not leaves. Similar up-regulation characteristics for stem growth and R soon after girdling have been observed in other girdling experiments (e.g., Daudet *et al.* 2005; Johnsen *et al.* 2007; López *et al.* 2015). These responses can be explained by changes in sink strength above and below the girdle. Accelerating D^{G+} and R will reduce NSC concentration in the phloem, thus stimulate continued loading and prevent accumulation of NSC in leaves. This mechanism does not involve hydrolysis of starch in leaves and explains the stable concentration of starch in leaves before and after girdling. As we have shown, D^{G+} close to the source was greatest during the day when NSC are assimilated, producing a clear rhythmicity of D^{G+} at the top of trees. NSC, including limited amounts of starch from storage at the top of trees were used to fuel high D^{G+} and R , while at the base the absence of ‘fresh’ NSC induced a significant depletion of both stored starch and available NSC to maintain some metabolic activity but not D^{G+} .

4.2 Effects of lateral fluxes

Previous theoretical and empirical studies have documented a synchronous radial movement of xylem and bark (e.g., Sevanto *et al.* 2011; Steppe *et al.* 2006, 2015; see also Scenario 1 in Fig. 1). This dynamic was interpreted as the result of diel rhythms of transpiration and associated changes in stem water potential that led to discharging and recharging of capacitive water stores. Field observations of asynchronous movement of the two tissues prompted the necessity for a refinement of this interpretation (Vandengehuchte *et al.* 2014; Zweifel *et al.* 2014; Pfautsch *et al.* 2015b; Mencuccini *et al.* 2017). In response, we have developed an empirically based method to separate most of the co-occurring fluxes in xylem and phloem from D^G (Mencuccini *et al.* 2013, 2017). Here we progressed the model from $D^{G_{\text{empir}}}$ to D^{G+} to fully account for viscoelastic movements in bark and xylem at high temporal resolution that have their origin in changes of

osmotic and hydraulic pressure in both tissue types.

High conditional and marginal coefficients of determination of our mixed effects model indicated good similarity between observed and modelled data outputs. The patterns, amplitudes and slightly offset sequence of oscillations in thickness of bark (dD_b) and xylem (dD_x) reflect our current understanding of the effects of changes in xylem pressure potential (Ψ_P) and osmotic potential (Ψ_{Π}) during the diel course of transpiration very well (e.g., Sevanto *et al.* 2003, 2011). Moreover, the changes in physiological functions after girdling, including the reduction of transpiration and shifts in the availability and use of NSC are all captured in our diel courses of dD_b and dD_x . It becomes clear that previous assessments of radial expansion and contraction of tree stems may have over- or under-estimated the magnitude of some effects, as they can act as a counterforce.

One example is the expansion of bark tissue during the night as consequence of capacitive recharge when pressure potential in xylem is close to zero (increasing $D_b^{\Psi_{\Pi\xi}}$ at stable $D_x^{\Psi_{\Pi\xi}}$). The amplitude of this change in bark thickness prior to girdling was around +60 μm at the base and top of the stems. Simultaneously, and driven by the dilution effect of water flowing back into the bark, tissue contraction of around -20 μm can be expected during the early hours of the night (decreasing $D_b^{\Psi_{\Pi\beta}}$ at increasing $D_x^{\Psi_{\Pi\xi}}$). These effects are in agreement with theoretical models that describe diurnal changes in turgor and osmotic potential in phloem and xylem (Hölttä *et al.* 2006, 2017). Measurements of dD_b alone that do not account for these changes would simply indicate a dimensional change of +40 μm . When assessing these effects during the post-girdling phase, it is clear that capacitive recharge and associated expansion of D_b is reduced below and above the girdle, reflecting the reduction in negative pressure exerted by the xylem in response to reduced rates of transpiration. The altered NSC dynamics result in a continuous contraction of D_b during the night below the girdle in response to the decline in NSC. Yet, at the same time D_b above the girdle continuously expands, potentially in response to accumulation of NSC in bark tissue that are not used to fuel D^{G+} (irreversible radial growth remains low during the night in the post-girdling phase, see Fig. 4f). Other similarly complex examples of counterforce effects can be deduced from our Figures 6 and 7.

The rhythmic pattern of high and low growth rates at the top of trees during the day and low growth during the night at the top of trees is not unusual. Using gene expression techniques, Solomon *et al.* (2010) provided evidence that stem growth in eucalypts is not necessarily a linear process limited to night-time hours. However, documenting a simultaneous occurrence of continuous growth at the stem base and a rhythmic growth pattern at the top of trees provides an important step forward in our understanding of the dynamic relationships between sources and sinks of NSC.

5. Conclusion

This work has refined our understanding of radial transport dynamics in tree stems. Girdling was used to generate experimental data to derive a detailed mechanistic model, that disentangles dimensional changes driven by cell expansion, hydraulic pressure, osmotic potential and radial transport processes in xylem and bark over 24-hour periods. In contrast to the paradigm that radial growth of stems mostly occurs during the night, we found that growth of *E. tereticornis* was continuous during day and night. Moreover, we documented asynchrony, where xylem expansion was greatest during the mid-day and bark expansion was greatest at night-time. Girdling accelerated stem growth above the girdle, particularly during the daytime, suggesting that increased carbon supply (including NSC) plays a critical role in the regulation of diurnal changes in stem diameter due to osmotic adjustment in bark and in xylem ray cells. Based on the observed responses to girdling, we devised a novel regulatory framework that helps explain patterns of contraction and expansion of bark and xylem. Applying this mechanistic model to better understand the hydraulic-metabolite interdependent processes that generate irreversible growth in stems of other tree species would be the logical next step to better understand the radial daily growth in trees more broadly.

6. Acknowledgements

The authors thank Burhan Amiji and Renee Smith for their technical support at the Whole Tree Chamber Research Facility. Sune Linder (Swedish University for Agricultural Sciences) is thanked for providing the

Whole-Tree Chamber Facility to the Hawkesbury Institute for the Environment (Western Sydney University, Australia). This research was supported by the Australian Research Council (Discovery, DP140103415), a New South Wales government Climate Action Grant (NSW T07/CAG/016), the Hawkesbury Institute for the Environment, and Western Sydney University.

7. Author contributions

SP, MT, PM, DT and MM designed the experiment. SP, MA, JD, CB and MT conducted the experiments and collected data. SP and MM evaluated the data. MM computed the model. SP produced the final draft of the manuscript with substantial inputs from VRD, DT and MM.

8. References

- Appel H.M., Arnold T.M. & Schultz J.C. (2012) Effects of jasmonic acid, branching and girdling on carbon and nitrogen transport in poplar. *New Phytologist* **195** , 419–426.
- Asao S. & Ryan M.G. (2015) Carbohydrate regulation of photosynthesis and respiration from branch girdling in four species from wet tropical rainforest trees. *Tree Physiology* **35** , 608–620.
- Avramidis S. (2007) Bound water migration in wood. Contribution to COST E15: Advances in the drying of wood. Department of Wood Science, The University of British Columbia, Vancouver, Canada. 27p.
- Barton C.V.M., Ellsworth D.S., Medlyn B.E., Duursma R.A., Tissue D.E., Adams M.A., ... Linder S. (2010) Whole-tree chambers for elevated atmospheric CO₂ experimentation and tree scale flux measurements in south-eastern Australia: The Hawkesbury Forest Experiment. *Agricultural and Forest Meteorology* **150** , 941–951.
- Binkley D., Stape J.L., Takahashi E.N. & Ryan M.G. (2006) Tree-girdling to separate root and heterotrophic respiration in two *Eucalyptus* stands in Brazil. *Oecologia* **148** , 447–454.
- Chan T., Hölttä T., Beringer F., Mäkinen H., Njöd P., Mencuccini M. & Nikinmaa E. (2016) Separating water-potential induced swelling and shrinking from measured radial stem variations reveals a cambial growth and osmotic concentration signal. *Plant, Cell and Environment* **39** , 233–244.
- Comas L.H. & Eissenstat D.M. (2004) Linking fine root traits to maximum potential growth rate among 11 mature temperate tree species. *Functional Ecology* **18** , 388–397.
- Cosgrove D.J. 2005. Growth of the plant cell wall. *Nature Reviews Molecular Cell Biology* **6** , 850–861.
- Cuny H., Rathgeber C.B.K., Frank D., Fonti P., Mäkinen H., Prislan P., ... Fournier M. (2015) Woody biomass production lags stem-girth increase by over one month in coniferous forests. *Nature Plants* , doi: 10.1038/nplants.2015.160.
- Daudet F.-A., Améglio T., Cochard H., Archilla O. & Lacoite A. (2005) Experimental analysis of the role of water and carbon in tree stem diameter variations. *Journal of Experimental Botany* **56** , 135–144.
- De Schepper V. & Steppe K. (2011) Tree girdling responses simulated by a water and carbon transport model. *Annals of Botany* **108** , 1147–1154.
- De Swaef T., Driever S.M., Van Meulebroek L., Vanhaecke L., Marcelis L.F.M. & Steppe K. (2013) Understanding the effect of carbon status on stem diameter variations. *Annals of Botany* **111** , 31–46.
- Domec J.-C. & Pruyn M.L. (2008) Bole girdling affects metabolic properties and root, trunk and branch hydraulics of young ponderosa pine trees. *Tree Physiology* **28** , 1493–1504.
- Drake J.E., Tjoelker M.G., Aspinwall M.J., Reich P.B., Barton C.V.M., Medlyn B.E. & Duursma R. (2016) Does physiological acclimation to climate warming stabilize the ratio of canopy respiration to photosynthesis? *New Phytologist* **211** , 850–863.

- Drake J.E., Vårhammar A., Kumarathunge D., Medlyn B.E., Pfautsch S., Reich P.B., ... Tjoelker M.G. (2017) A common thermal niche among geographically diverse populations of the widely distributed tree species *Eucalyptus tereticornis* : no evidence for adaptation to climate of origin. *Global Change Biology* **23** , 5069–5082.
- Epron D., Cabral O.M.R., Laclau J.-P., Dannoura M., Packer A.P., Battie-Laclau P., ... Nouvellon Y. (2016) In situ $^{13}\text{CO}_2$ pulse labelling of field-grown eucalypt trees revealed the effect of potassium nutrition and throughfall exclusion on phloem transport of photosynthetic carbon. *Tree Physiology* **36** , 6–21.
- Fromm J. (ed) (2013) Cellular aspects of wood formation. Springer-Verlag Berlin, 264 p.
- Furze M.E., Trumbore S. & Hartmann H. (2018) Detours on the phloem sugar highway: stem carbon storage and remobilization. *Current Opinion in Plant Biology* **43** , 89–95.
- Hartmann H. & Trumbore S. (2016) Understanding the roles of non-structural carbohydrates in forest trees – from what we can measure to what we want to know. *New Phytologist* **211** , 386–403.
- Hölttä T., Vesala T., Sevanto S., Perämäki M. & Nikinmaa E. (2006) Modelling xylem and phloem water flows in trees according to cohesion theory and Münch hypothesis. *Trees* **20** , 67–78.
- Hölttä T., Mencuccini M. & Nikinmaa E. (2009) Linking phloem function to structure: Analysis with a coupled xylem-phloem transport model. *Journal of Theoretical Biology* **259** , 325–337.
- Hölttä T., Mäkinen H., Nöjd P., Mäkelä A. & Nikinmaa E. (2010) A physiological model of softwood cambial growth. *Tree Physiology* **30** , 1235–1252.
- Hölttä T., Lintunen A., Chan T., Mäkelä A. & Nikinmaa E. (2017) A steady-state stomatal model of balanced leaf gas exchange, hydraulics and maximal source-sink flux. *Tree Physiology* **37** , 851–868.
- Hogberg P., Nordgren A. & Buchmann N. (2001) Large-scale forest girdling shows that current photosynthesis drives soil respiration. *Nature* **411** , 789–792.
- Johnsen K., Maier C.A., Sanchez F., Anderson P., Butnor J., Waring R. & Linder S. (2007) Physiological girdling of pine trees via phloem chilling: proof of concept. *Plant, Cell and Environment* **30** , 128–134.
- Kurtzmann Jr. R.H. (1966) Xylem sap flow as affected by metabolic inhibitors and girdling. *Plant Physiology* **41** , 641–646.
- López R., Brossa R., Gil L. & Pita P. (2015) Stem girdling evidences a trade-off between cambial activity and sprouting and dramatically reduces plant transpiration due to feedback inhibition of photosynthesis and hormonal signalling. *Frontiers in Plant Science* **6** , 1–13.
- Maier C.A., Johnsen K.H., Clinton B.D. & Ludovici K.H. (2010) Relationships between stem CO_2 efflux, substrate supply, and growth in young loblolly pine trees. *New Phytologist* **185** , 502–513.
- Martínez-Vilalta J., Sala A., Asensio D., Galiano L., Hoch G., Palacio S., ... Lloret F. (2016) Dynamics of non-structural carbohydrates in terrestrial plants: a global synthesis. *Ecological Monographs* , doi: 10.1002/ecm.1231.
- McNaughton K.G. & Jarvis P.G. (1991) Effects of spatial scale on stomatal control of transpiration. *Agricultural and Forest Meteorology* **54** , 279–301.
- Mencuccini M., Hölttä T., Sevanto S. & Nikinmaa E. (2013) Current measurements of change in the bark and xylem diameters of trees reveal a phloem-generated turgor signal. *New Phytologist* **198** , 1143–1154.
- Mencuccini M., Salmon Y., Mitchell P., Hölttä T., Choat B., Meir P., ... Pfautsch S. (2017) An empirical method that separates irreversible stem radial growth from bark water content changes in trees: theory and case studies. *Plant, Cell and Environment* **40** , 290–303.

- Nebauer S.G, Renau-Morata B., Guardiola J.L. & Molina R.-V. (2011) Photosynthesis down-regulation precedes carbohydrate accumulation under sink limitation in *Citrus* . *Tree Physiology* **31** , 169–177.
- Oberhuber W., Gruber A., Lethaus G., Winkler A. & Wieser G. (2017) Stem girdling indicates prioritized carbon allocation to the root system at the expense of radial stem growth in Norway spruce under drought conditions. *Environmental and Experimental Botany* **138** , 109–118.
- Pfautsch S., Hölttä T. & Mencuccini M. (2015a) Hydraulic functioning of tree stems – fusing ray anatomy, radial transfer and capacitance. *Tree Physiology* **35** , 706–722.
- Pfautsch S., Renard J., Tjoelker M.G. & Salih A. (2015b) Phloem as capacitor: Radial transfer of water into xylem of tree stems occurs via symplastic transport in ray parenchyma. *Plant Physiology* **167** , 963–971.
- Pfautsch S. (2016) Hydraulic anatomy and function of trees – basics and critical developments. *Current Forestry Reports* **2** , 236–248.
- Poorter H., Remkes C. & Lambers H. (1990) Carbon and nitrogen economy of 24 wild species differing in relative growth rate. *Plant Physiology* **94** , 621–627.
- Salleo S., Lo Gullo M.A., Trifilò P. & Nardini A. (2004) New evidence for a role of vessel-associated cells and phloem in the rapid xylem refilling of cavitated stems of *Laurus nobilis* L. *Plant, Cell and Environment* **27** , 1065–1076.
- Schrader J., Moyle R., Bhalerao R., Hertzberg M., Lundeberg J., Nilsson P. & Bhalerao R.P. (2004) Cambial meristem dormancy in trees involves extensive remodelling of the transcriptome. *Plant Journal* **40**, 173–187
- Sellier D. & Mammeri Y. (2019) Diurnal dynamics of phloem loading: theoretical consequences for transport efficiency and flow characteristics. *Tree Physiology* **39** , 300–311.
- Sellin A., Niglas A., Öunapuu E. & Karusion A. (2013) Impact of phloem girdling on leaf gas exchange and hydraulic conductance in hybrid aspen. *Biologia Plantarum* **57** , 531–539.
- Sevanto S., Vesala T., Perämäki M. & Nikinmaa E. (2003) Sugar transport together with environmental conditions controls time lags between xylem and stem diameter changes. *Plant, Cell and Environment* **26** , 1257–1265.
- Sevanto S., Hölttä T. & Holbrook N.M. (2011) Effects of the hydraulic coupling between xylem and phloem on diurnal phloem diameter variation. *Plant, Cell and Environment* **34** , 690–703.
- Solomon O.L., Beger D.K. & Myburg A.A. (2010) Diurnal and circadian patterns of gene expression in the developing xylem of *Eucalyptus* trees. *South African Journal of Botany* **76** , 425–439.
- Steppe K., De Pauw D.J.W., Lemeur R. & Vanrolleghem P.A. (2006) A mathematical model linking tree sap flow dynamics to daily stem diameter fluctuations and radial stem growth. *Tree Physiology* **26** , 257–273.
- Steppe K., Sterck F. & Deslauriers A. (2015) Diel growth dynamics in tree stems: linking anatomy and ecophysiology. *Trends in Plant Science* **20** , 335–343.
- Tissue D.T. & Wright S.J. (1995) Effect of seasonal water availability on phenology and the annual shoot carbohydrate cycle of tropical forest shrubs. *Functional Ecology* **9** , 518–527.
- Tjoelker M.G., Oleksyn J. & Reich P.B. (1999) Acclimation of respiration to temperature and CO₂ in seedlings of boreal tree species in relation to plant size and relative growth rate. *Global Change Biology* **5** , 679–691.
- Tjoelker M.G., Craine J.M., Wedin D., Reich P.B. & Tilman D. (2005) Linking leaf and root trait syndromes among 39 grassland and savannah species. *New Phytologist* **167** , 493–508.
- Tombesi S., Day K.R., Johnson R.S., Phene R. & DeJong T.M. (2014) Vigour reduction in girdled peach trees is related to lower midday stem water potentials. *Functional Plant Biology* **41** , 1336–1341.

Treydte K., Lehmann M.M., Wyszczesany T & Pfautsch S. (2021) Radial and axial water movement in adult trees recorded by stable isotope tracing. *Tree Physiology* , accepted.

Ueda M., Shibata, E., Fukuda H., Sano A. & Waguchi Y. (2014) Girdling and tree death: lessons from *Chamaecyparis pisifera*. *Canadian Journal of Forest Research* **44** , 1133–1137.

Vandengehuchte M.W., Guyot A., Hubau M., De Groote S.R.E., De Braedemaeker N.F.J. ... Steppe K. (2014) Long-term versus daily stem diameter variation in co-occurring mangrove species: environmental versus ecophysiological drivers. *Agricultural and Forest Meteorology* **192-193** , 51–58.

Yang Q., Zhang W., Li R., Zheng W., Yang Y., Xu M. ... Wang S. (2019) Effects of girdling on stem CO₂ efflux and its temperature sensitivity in Chinese fir and sweetgum trees. *Agricultural and Forest Meteorology* **268** , 116–123.

Zweifel R., Item H. & Häslér R. (2001) Link between diurnal stem radius changes and tree water relations. *Tree Physiology* **21** , 869–877.

Zweifel R., Drew D., Schweingruber F. & Downes G.M. (2014) Xylem as the main origin of stem radius changes in *Eucalyptus* .*Functional Plant Biology* **41** , 520–534.

Zwieniecki M.A., Melcher P.J., Feild T.S. & Holbrook N.M. (2004) A potential role for xylem-phloem interactions in the hydraulic architecture of trees: effects of phloem girdling on xylem hydraulic conductance. *Tree Physiology* **24** , 911-917.

Figures

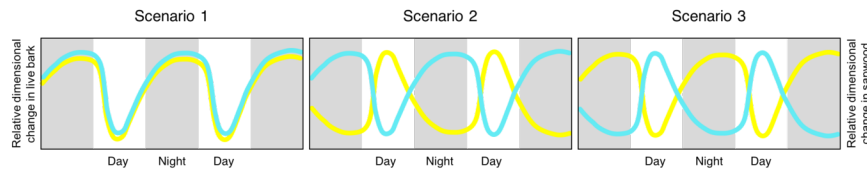


Figure 1. Simplified schematic representation of observed movement in live bark (yellow) and sapwood (turquoise) of trees. Scenario 1: *synchronous* movement, where live bark and sapwood contract in parallel during the day and expand in parallel during the night (observed in maple, birch and oak, Sevanto *et al.* (2011)). Scenario 2: *a-synchronous* movement, where live bark expands during the day, while sapwood contracts (observed in *Eucalyptus globulus* , Zweifel *et al.* (2014)) with the reversal of this pattern during the night. Scenario 3: *a-synchronous* movement, where live bark contracts during the day, while sapwood expands (observed in *Eucalyptus saligna* , Pfautsch *et al.* (2015a)), *E. tereticornis* (this study). Note, irreversible radial growth is excluded in these schematic drawings.

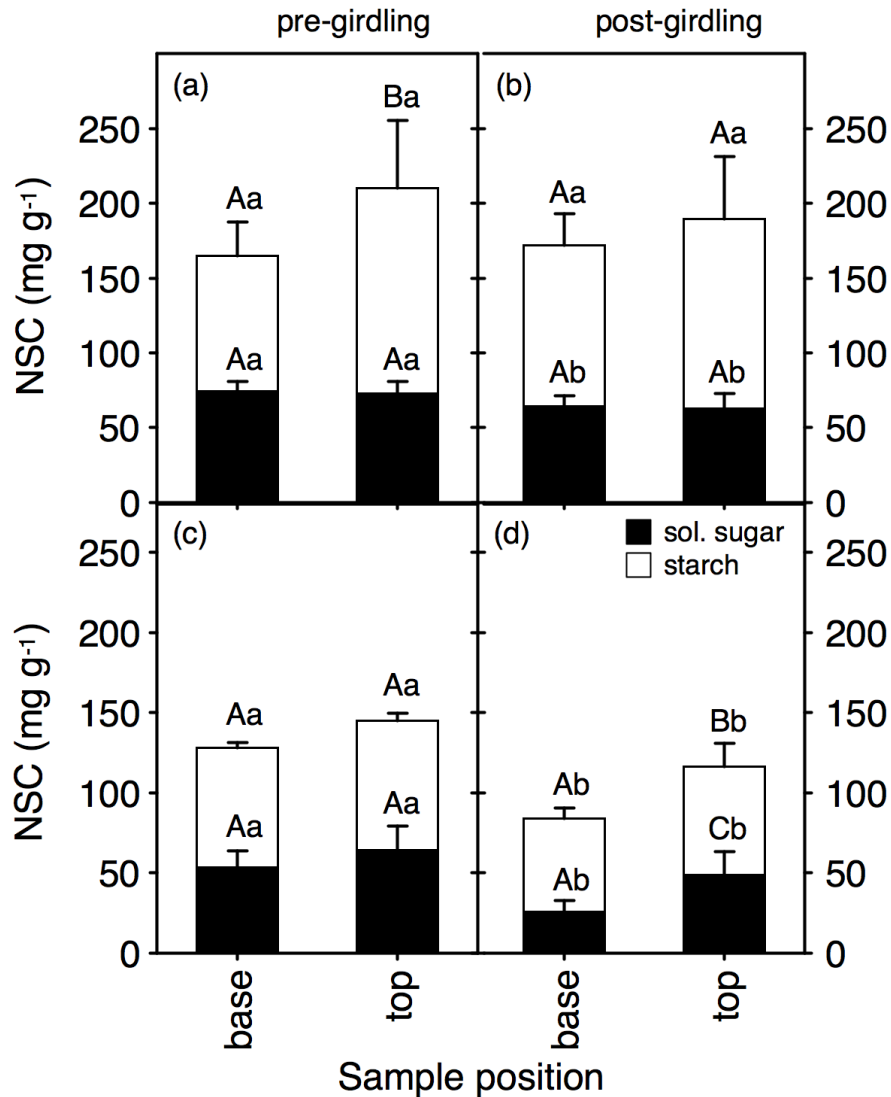


Figure 2. Concentration of non-structural carbohydrates (NSC) pre- and post-girdling. NSC were measured at (a) leaves at pre-girdling; (b) leaves at post-girdling; (c) bark at pre-girdling; and (d) bark at post-girdling in *Eucalyptus tereticornis* trees (n = 6). Bars are split to separately show concentrations of starch (clear) and soluble sugars (black). Tissues were collected at 10 am on 16 May (pre-girdling) and 25 May 2015 (post-girdling). Please refer to text for explanation of sample positions. Different capital letters indicate significant differences among the two sampling positions. Different lower-case letters indicate significant differences between tissues collected from the same sample position before and after girdling. Significance was given when $p < 0.05$. Error bars show +1 Standard Deviation.

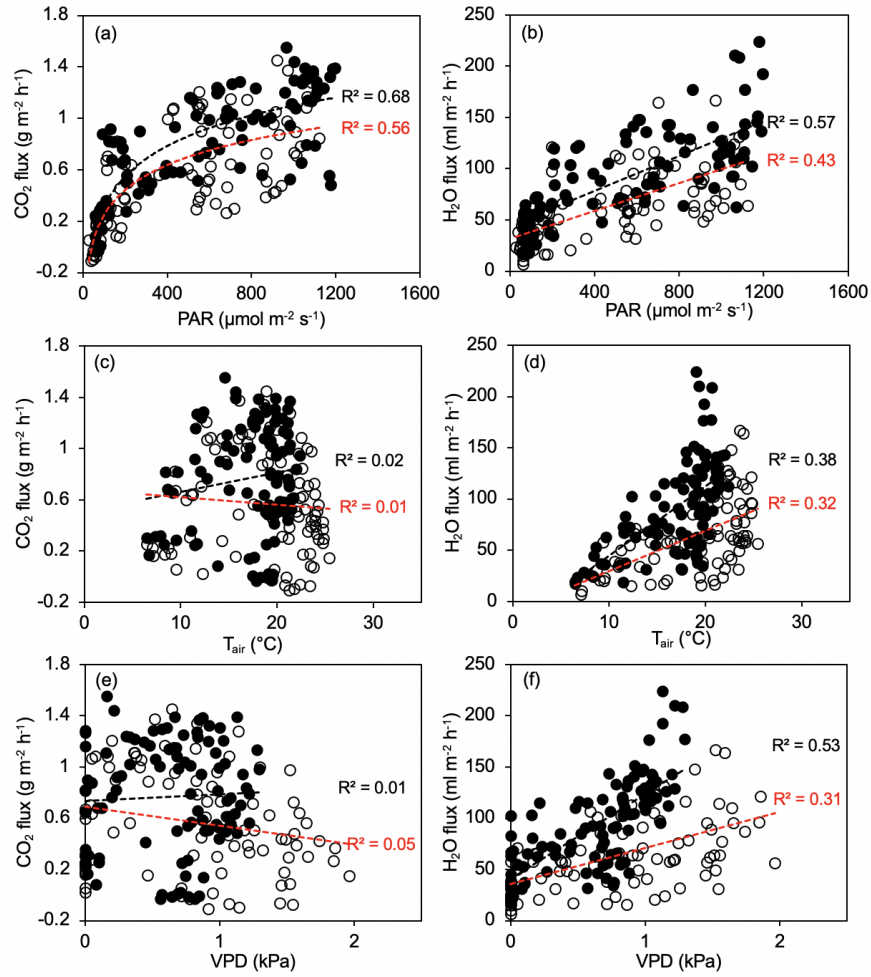


Figure 3. Relationships between environmental conditions and whole-tree gas fluxes before (dots, dashed black line) and after girdling (circles, dashed red line) of *Eucalyptus tereticornis* trees ($n = 6$). Data represent hourly measurements (07:00-16:00 h) recorded from 6 to 15 May (pre-girdling) and 17-24 May 2014 (post-girdling). Left-side panels show responses of CO₂ fluxes and right-side panels those of H₂O fluxes to environmental conditions. Environmental conditions are photosynthetic active radiation (PAR, top panels), air temperature (T_{air}, middle panels) and vapour pressure deficit of the atmosphere (VPD, bottom panels). Best fit functions and their coefficients of determination are shown in each panel.

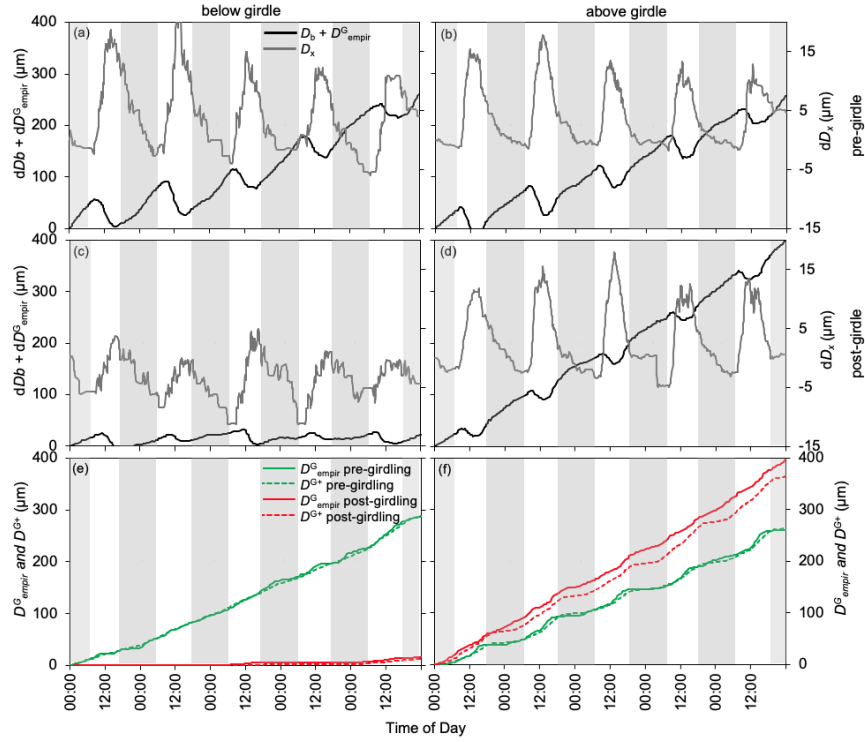


Figure 4. Radial movement measured on live bark and sapwood in six *Eucalyptus tereticornis* trees. Left-side panels show data were recorded below the girdle, right-side panels show data recorded above the girdle before (top panels; 6-10 May) and after (bottom panels; 20-24 May) all bark was removed 60 cm above the stem base. Data recorded on live bark (black line) contain the combined signals of reversible (dD_b) and irreversible (dD^G_{empir}) expansion of live bark and the cambial region (see text for more details), while those recorded on sapwood (grey line) represent reversible expansion of xylem (dD_x) only. Panels (e) and (f) depict irreversible growth of stems based on interpolated dendrometer measurements that contain hydraulic and osmotic signals (D^G_{empir}) and those that have been stripped of these signals (D^{G+}). Grey sections indicate night-time (19:00-07:00 h).

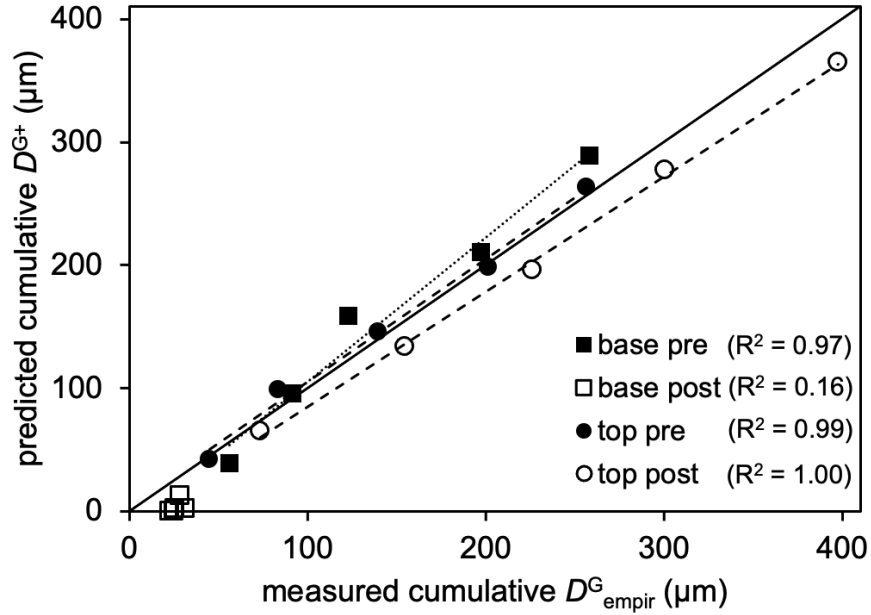


Figure 5. Measured cumulative irreversible growth (D^G_{empir}) against modelled cumulative irreversible growth (D^{G+}) in *Eucalyptus tereticornis* trees ($n = 6$). Data represents irreversible growth for five consecutive days pre-girdling (solid symbols; 6-10 May 2014) and post-girdling (open symbols; 20-24 May 2014) at two different positions along the stem (base = below the girdle; top = above the girdle). Solid line depicts 1:1 relationship; dotted and dashed lines show linear fits. Coefficients of determination (R^2) are shown for each relationship.

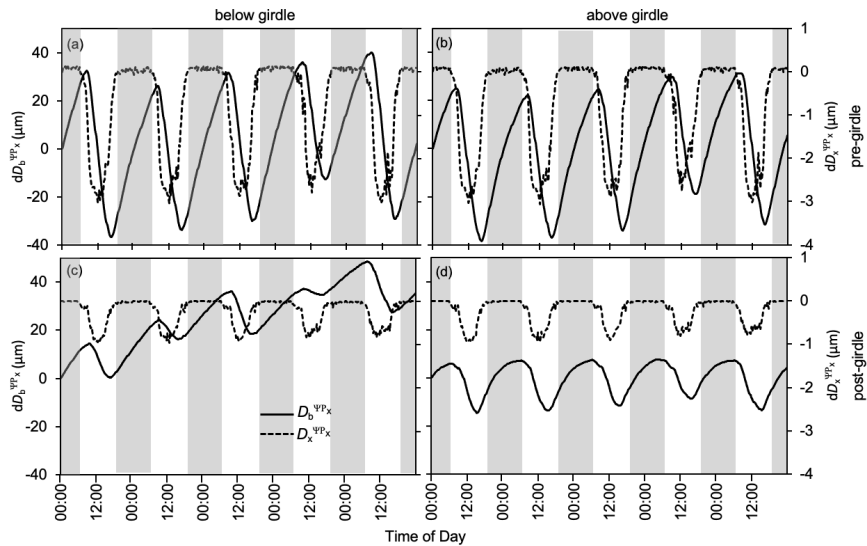


Figure 6. Diel courses of simultaneous radial viscoelastic changes in live bark (dD_b) and xylem (dD_x) tissue as a result of change in xylem pressure potential (ΨPx) in *Eucalyptus tereticornis* trees ($n = 6$). Left-side panels show viscoelastic changes below the girdle, right-side panels show these changes above the girdle; top panels show these changes before (6-10 May) and after (bottom panels; 20-24 May) girdling of

tree stems. Output was generated using the mechanistic model described in Material and Methods. Grey sections indicate night-time (19:00–07:00 h).

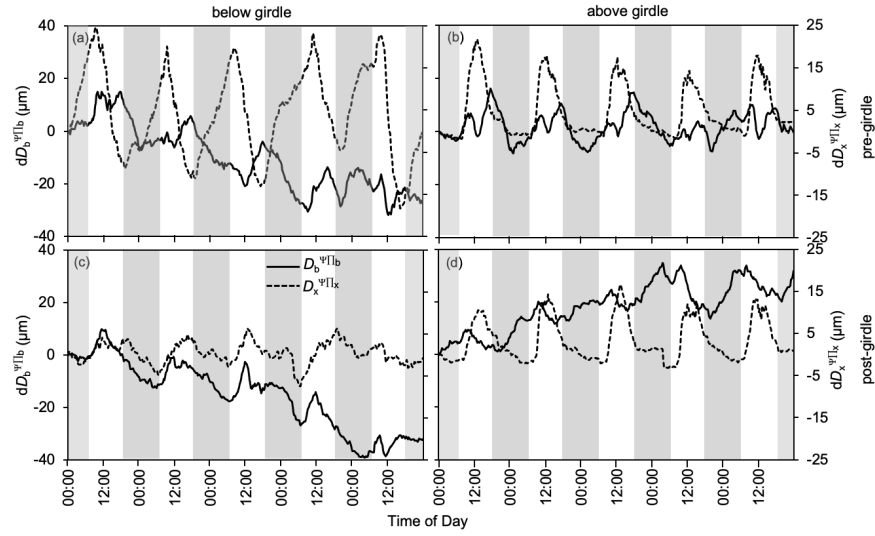


Figure 7. Diel courses of simultaneous radial viscoelastic changes in live bark (dD_b) and xylem (dD_x) tissue as a result of change in osmotic pressure potential in live bark (Ψ_{IIb}) and xylem (Ψ_{IIx}) in *Eucalyptus tereticornis* trees ($n = 6$). Left-side panels show viscoelastic changes below the girdle, right-side panels show these changes above the girdle; top panels show these changes before (6-10 May) and after (bottom panels; 20-24 May) girdling of tree stems. Output was generated using the mechanistic model described in Material and Methods. Grey sections indicate night-time (19:00–07:00 h).

Tables

Table 1. Specifications of six *Eucalyptus tereticornis* trees used in the experiment. Abbreviations: H_t = total tree height; D_{sb} = basal stem diameter; LA = total leaf area; H_d = height of dendrometer installation; D_b = stem diameter at dendrometer installation at the stem base; T_b = bark thickness at dendrometer installation. Data for T_b are means of four measurements around the stem circumference ± 1 Standard Deviation. Data are shown for dendrometers installed at the base and top of stems.

| Tree # | H_t (m) | D_{sb} (mm) | LA (m^2) | Base | Base | Base | Top | Top | Top |
|--------|-----------|---------------|--------------|-----------|------------|-------------------|-----------|------------|-------------------|
| | | | | H_d (m) | D_d (mm) | T_b (mm) | H_d (m) | D_d (mm) | T_b (mm) |
| 1 | 8.46 | 93 | 17.88 | 0.54 | 66 | 6.3 (± 1.0) | 2.59 | 48 | 4.5 (± 0.6) |
| 2 | 8.65 | 78 | 11.03 | 0.54 | 59 | 6.0 (± 0.0) | 2.74 | 48 | 4.5 (± 0.6) |
| 3 | 8.71 | 94 | 26.75 | 0.61 | 72 | 6.0 (± 1.2) | 3.57 | 51 | 4.7 (± 0.5) |
| 4 | 9.18 | 89 | 17.42 | 0.55 | 69 | 5.7 (± 0.5) | 4.39 | 51 | 4.3 (± 0.5) |
| 5 | 8.02 | 91 | 13.78 | 0.69 | 63 | 7.2 (± 1.3) | 3.50 | 48 | 3.8 (± 0.5) |
| 6 | 9.34 | 103 | 21.92 | 0.68 | 69 | 7.8 (± 0.5) | 3.65 | 48 | 5.3 (± 0.5) |

Table 2. Effect of girdling on dark respiration of leaves, branches and stems of *Eucalyptus tereticornis* trees ($n = 6$). Rates of respired CO_2 from leaves and branches ($nmol\ g^{-1}\ s^{-1}$) measured in the dark at a constant 15 °C before (13 May) and after girdling (22 May) and results of a one-way repeated measures analysis of variance (RM-ANOVA) are shown. RM-ANOVA for whole-tree data is not included due to very large variation among trees (see text for more details). Data in parenthesis are ± 1 Standard Deviation.

| Respiration | Leaves | Branches |
|------------------------------------|---|---|
| <i>Pre-girdling</i> | nmol CO ₂ g ⁻¹ DW s ⁻¹ 3.38 (±1.15) | nmol CO ₂ g ⁻¹ DW s ⁻¹ 1.33 (±0.24) |
| <i>Post-girdling</i> | 3.43 (±0.75) | 1.89 (±0.30) |
| One-way RM-ANOVA (Leaves) | One-way RM-ANOVA (Leaves) | One-way RM-ANOVA (Leaves) |
| <i>Source</i> | SoS | <i>df</i> |
| <i>between-subjects</i> | 15.48 | 11 |
| <i>Sampling date</i> | 0.02 | 1 |
| One-way RM-ANOVA (Branches) | One-way RM-ANOVA (Branches) | One-way RM-ANOVA (Branches) |
| <i>Source</i> | SoS | <i>df</i> |
| <i>between-subjects</i> | 0.97 | 11 |
| <i>Sampling date</i> | 1.89 | 1 |

Table 3. Model coefficients, 95% confidence intervals, significance levels and R² (representing the percentage of explained variance by fixed and random factors (conditional, R²_c) and by fixed factors (marginal, R²_m) for the linear mixed effect model that aims to separate irreversible cambial growth (D^{G+}) from changes caused by radial hydraulic and osmotic changes (including radial transfer of osmotica) prior to, and after girdling. For the model prior to girdling, sensor position was not significant; for the model following girdling, the positions below and above were significantly different and there were significant interactions between sensor position and all four variables of Equation 1. Using tree number, sample position and sampling date (random effects) and D_x and D_b (fixed factors), our model was able to explain a large proportion of variation introduced by radial hydraulic capacitance.

Model prior to girdling

| | α | β | γ |
|---------------------------------|---------------------------------|---------------------------------|---------------------------------|
| Mean | 0.0190 | 335.83 | 3.74 |
| 95% CI | 0.183 – 0.0197 | 310.80 - 360.85 | 3.71-3.79 |
| P-level | <2E-16 | <2E-16 | <2E-16 |
| Model following girdling | Model following girdling | Model following girdling | Model following girdling |
| | α | β | γ |
| <i>above point of girdling</i> |
| Mean | 0.0419 | 80.41 | 1.57 |
| 95% CI | 0.0364 - 0.0475 | 50.05 – 110.76 | 1.02 – 2.12 |
| P-level | <2E-16 | <2E-16 | <2E-16 |
| <i>below point of girdling</i> |
| Mean | 0.0055 | 618.18 | 1.57 |
| 95% CI | 0.0030-0.0079 | 261.09-975.28 | 1.02-2.12 |
| P-level | <2E-16 | <2E-16 | <2E-16 |